Atmos. Meas. Tech. Discuss., 7, 7923–7962, 2014
www.atmos-meas-tech-discuss.net/7/7923/2014/
doi:10.5194/amtd-7-7923-2014


Atmospheric Measurement Techniques Discussions
Open Access

This discussion paper is/has been under review for the journal Atmospheric Measurement Techniques (AMT). Please refer to the corresponding final paper in AMT if available.

# Tropospheric ozone and ozone profiles retrieved from GOME-2 and their validation

**G. M. Miles**[1], **R. Siddans**[1], **B. J. Kerridge**[1], **B. G. Latter**[1], **and N. A. D. Richards**[2]

[1]Remote Sensing Group, STFC Rutherford Appleton Laboratory, Harwell Oxford, UK
[2]School of Earth and Environment, University of Leeds, Leeds, UK

Received: 10 June 2014 – Accepted: 10 July 2014 – Published: 31 July 2014

Correspondence to: G. M. Miles (georgina.miles@stfc.ac.uk)

Published by Copernicus Publications on behalf of the European Geosciences Union.

## Abstract

This paper describes and assesses the performance of the RAL (Rutherford Appleton Laboratory) ozone profile retrieval scheme for the Global Ozone Monitoring Experiment 2 (GOME-2) with a focus on tropospheric ozone. Developments to the scheme since its application to GOME-1 measurements are outlined. These include the approaches developed to account sufficiently for UV radiometric degradation in the Hartley band and for inadequacies in knowledge of instrumental parameters in the Huggins bands to achieve the high precision spectral fit required to extract information on tropospheric ozone.

The assessment includes a validation against ozonesondes (sondes) sampled worldwide over two years (2007–2008). Standard deviations of the ensemble with respect to the sondes are considerably lower for the retrieved profiles than for the a priori, with the exception of the lowest sub-column. Once retrieval vertical smoothing (averaging kernels) has been applied to the sonde profiles there is a retrieval bias of 6 % (1.5 DU) in the lower troposphere, with smaller biases in the sub-columns above. The bias in the troposphere varies with latitude. The retrieval underestimates lower tropospheric ozone in the Southern Hemisphere (SH) (15–20 % or ~ 1–3 DU) and overestimates it in the Northern Hemisphere (NH) (10 % or 2 DU).

The ability of the retrieval to represent the geographical distribution of lower tropospheric ozone, globally (rather than just ozonesonde launch sites) is demonstrated through agreement with the chemistry transport model TOMCAT. For a monthly mean of cloud-cleared GOME-2 pixels, a correlation of 0.66 is found between the retrieval and TOMCAT sampled accordingly, with a bias of 0.7 Dobson Units. GOME-2 estimates higher concentrations in NH pollution centres but lower ozone in the Southern Ocean and South Pacific, which is consistent with the comparison to ozonesondes.






AMTD
7, 7923–7962, 2014

Tropospheric ozone and ozone profiles retrieved from GOME-2 and their validation

G. M. Miles et al.

## 1 Introduction

Ozone is an important atmospheric trace gas, absorbing ultraviolet (UV) radiation from the sun that would otherwise damage the cells of living organisms at the Earth's surface. In the stratosphere, where approximately 90 % of ozone is found, the vertical distribution determines heating rates and thereby also dynamics. Stratospheric ozone is produced by photolysis of molecular oxygen at shorter UV wavelengths and destroyed by catalytic cycles involving nitrogen, hydrogen and halogen radicals. In the troposphere, ozone is produced though complex reaction pathways involving nitrogen oxides ($NO_x$) and volatile organic compounds (VOCs). Ozone is also introduced by exchange from the stratosphere, particularly at mid-latitudes. As a secondary pollutant from anthropogenic and biomass burning sources, it is an environmental hazard particularly in urban environments because it is a lung irritant. High levels of ozone have been linked to increased mortality/excess deaths when associated with localised heat wave events (Gryparis et al., 2004). Tropospheric ozone can be damaging to agriculture by increasing the failure rate of crops (Holloway et al., 2012). For these reasons, it is vitally important to monitor ozone in the troposphere as well as the stratosphere, but in situ surface observations and ozonesondes are sparse and heavily favour the Northern Hemisphere.

Tropospheric ozone is also a greenhouse gas. The uncertainty in estimates of radiative forcing from tropospheric ozone is as large as that associated with the non-well mixed greenhouse gases (IPCC, 2013) and as such good knowledge of the atmospheric concentration of tropospheric ozone is required. This uncertainty remains in part due to the reliance on atmospheric models and their spread, in addition to uncertainty about pre-industrial ozone amount. Estimates do not currently incorporate any information from satellites (IPCC 2013). An accurate, contemporary distribution of tropospheric ozone from satellites would help to verify chemistry transport models (CTM) and coupled chemistry-climate models (CCMs), and hence their estimates of radiative forcing and the forward projections by CCMs. The MetOp series and its



Discussion Paper | Discussion Paper | Discussion Paper | Discussion Paper |

AMTD

7, 7923–7962, 2014

Tropospheric ozone and ozone profiles retrieved from GOME-2 and their validation

G. M. Miles et al.

successor MetOp-SG/Sentinel 5 have the potential to monitor tropospheric as well as stratospheric ozone in the decades to come.

The total atmospheric column of ozone has been measured historically via UV nadir-viewing sensors (e.g. BUV, SBUV, TOMS, SBUV-2, GOME, SCIAMACHY, OMI and GOME-2), with accuracies typically between 0.5–2 % (Klenk et al., 1982; Loyola et al., 2011; van Roozendael et al., 2012; Sofieva et al., 2012 and references therein). Ozone profiles have also been produced from UV nadir-sounders (e.g. Bhartia et al., 1996), however, retrieving tropospheric ozone presents a significant challenge, because ~ 90 % of atmospheric ozone resides in the stratosphere above. Tropospheric columns have been derived by subtracting an estimate of the stratospheric component from the measured total column, using knowledge of the tropopause height and making assumptions about the ozone profile shape (e.g. Fishman and Larsen, 1987; Schoeberl et al., 2007; Ziemke et al., 2011). Tropospheric columns have also been derived in the tropics by differencing total columns in cloud-free pixels from those in nearby pixels with thick/high convective cloud (Valks et al., 2014). However, as suitable occurrences are sparse, only monthly averages are useful. Direct retrieval of tropospheric information from temperature-dependent spectral structure in the Huggins Bands (320–345 nm) was first proposed by Chance (1997) and has been exploited by several schemes (Munro et al., 1997; Liu et al., 2005, 2010; Cai et al., 2012), applied to the Global Ozone Monitoring Experiment (GOME) class of instruments.

Infrared nadir-viewing spectrometers offer complementary vertical sensitivity to tropospheric ozone, as demonstrated by the Tropospheric Emission Spectrometer (TES) (Nassar et al., 2008) and the Infrared Atmospheric Sounding Instrument (IASI) (Boynard et al., 2009).

Here, we describe and assess the performance of the RAL ozone profile retrieval scheme applied to GOME-2 measurements, with a particular focus on the troposphere. This scheme has been developed directly from that presented by Munro et al. (1997), which was the first to demonstrate retrieval of tropospheric ozone from space. Substantial improvements have been made to that algorithm and GOME-2, which was





AMTD
7, 7923–7962, 2014

launched on MetOp-A in 2006, also improves in certain respects upon its predecessor. The RAL ozone profile optimal estimation (OE) retrieval scheme was selected for the ESA Climate Change Initiative (CCI) (Plumber, 2009) after independent comparison to the GOME-2 operational ozone profile scheme (Keppens et al., 2014). It was selected principally because of the demonstrated sensitivity to tropospheric ozone and persistently higher number of degrees of freedom for signal (DFS).

In Sect. 2 of this paper, the GOME-2 instrument will be briefly introduced, before the RAL ozone profile scheme and the principal improvements since Munro et al. (1997) are described. In Sect. 3, an error assessment is described. Section 4 presents a validation of the ozone profile scheme against global ozonesondes and a comparison to tropospheric ozone distributions from a chemistry transport model. A summary is presented in Sect. 5.

## 2 RAL ozone profile retrieval algorithm

### 2.1 GOME-2 instrument

GOME-2 is a UV/vis spectrometer with four bands that cover the 240–790 nm interval contiguously with a spectral sampling of 0.11–0.22 nm and spectral resolution of 0.24–0.53 nm that was launched in 2006 aboard ESA's MetOp-A platform (Callies et al., 2000). MetOp has a local equator crossing time of 09:30 LST. Of principle use for the retrieval of atmospheric ozone are Bands 1 (240–315 nm) and 2 (310–403 nm), which incorporate the longwave side of the Hartley band (200–310 nm) and the Huggins (320–360 nm) bands. The Band 1a pixel size is 640 km (across-track) × 40 km (along-track). The nominal Band 1b and Band 2 pixel size is 80 km × 40 km (cf. 320 km × 40 km for GOME). In addition to earthshine spectra, GOME-2 also measures a direct sun spectrum once per day. A full description of the GOME-2 instrument is given within Callies et al. (2000).





AMTD
7, 7923–7962, 2014

## 2.2 Retrieval algorithm

The RAL ozone profile retrieval scheme is an optimal estimation (OE) algorithm (Rodgers, 1976, 2000) which uses prior information to constrain ill-posed problems such as profile retrievals from nadir-viewing satellite instruments. OE also provides an estimate of the errors associated with retrieved parameters.

The RAL algorithm is a three-step sequential retrieval, first performing a fit to the sun-normalised radiance spectrum in Band 1 (266–307 nm) to utilise information in the long-wave tail of the Hartley band. Band 1b spectra are averaged onto Band 1a spatial pixels to improve their signal to noise ratio. Ozone absorption and Rayleigh scattering coefficient both decrease strongly with wavelength across this interval, yielding information predominantly on the mid to upper stratospheric ozone profile. In addition to the ozone profile, the retrieved parameters are a wavelength-independent Lambertian effective surface albedo, detector dark (leakage) current (in raw signal units) and a wavelength mis-registration parameter for the earthshine spectra with respect to the direct-sun spectrum. Rotational Raman scattering is also accounted for by retrieving a scaling factor for the theoretically-calculated spectrum of in-filling by the (singly-scattered) Ring effect (as modelled via the approach of Joiner, 1995).

The second step is to retrieve an effective surface albedo at 336 nm in Band 2. This step is important because the effective albedo retrieved from the longest wavelengths (< 307 nm) in Band 1, is not appropriate in the Band 2 (323–335 nm) fit due to the differing fields of view (FoV). The retrieved ozone profile and its associated error covariance matrix from the Band 1 fit and the retrieved 336 nm effective albedo contribute to the prior information for the third and final fit in the Huggins Bands (323–335 nm).

The fit in Band 1 is a direct fit of the sun normalised radiance, $\boldsymbol{r}$, defined as:

$$\boldsymbol{r} = \frac{\boldsymbol{I}}{\boldsymbol{I}_0}\pi \qquad (1)$$

Where $\boldsymbol{I}$ is the measured earthshine radiance and $\boldsymbol{I}_0$ the direct-sun irradiance measurement. As such, accurate (< 1 %) radiometric calibration is required. GOME-2, as



AMTD
7, 7923–7962, 2014
Tropospheric ozone and ozone profiles retrieved from GOME-2 and their validation
G. M. Miles et al.
Title Page | Abstract | Introduction | Conclusions | References | Tables | Figures | Back | Close | Full Screen / Esc | Printer-friendly Version | Interactive Discussion
Discussion Paper | Discussion Paper | Discussion Paper | Discussion Paper

with GOME-1 and SCIAMACHY, has experienced degradation of the UV photometric throughput during its lifetime, the effects of which are greater for the shorter wavelengths (Lang et al., 2009; Lacan and Lang, 2011; Cai et al., 2012). To produce self-consistent global ozone distributions over the mission lifetime, it has been necessary to implement an empirical degradation correction to the Band 1 measurements, as outlined below in Sect. 2.3.1.

In order to obtain accurate information on tropospheric ozone, a high fitting precision in the Huggins Bands is required, $<0.1\,\%$ RMS. In order to achieve this, the Band 2 retrieval fits the differential wavelength structure arising from temperature-dependent vibration-rotational structure in ozone absorption, using the logarithm of the sun-normliased radiance, with a 4th order polynomial in wavelength subtracted in order to remove coarse scale artefacts in the spectrum[1] and reveal the fine-scale ozone differential spectral structure. This method of fitting differential spectral structure is somewhat analogous to the DOAS approach (Platt, 1994) and is robust against instrumental effects (including some aspects of the degradation). The stringent fitting precision requirement necessitates good knowledge of the instrument's slit function, which varies across Band 2. This is achieved by an off-line fit to each direct-sun spectrum, to retrieve a scaling factor to apply to slit function key data from pre-flight characterisation (Siddans et al., 2003). This is done on a daily basis because the slit functions are observed to change with time (seasonally and over shorter time periods) in association with thermal cycling of the instrument focal plane. This process is discussed further in Sect. 2.3.3.

The state vector for the Band 2 retrieval step is composed of a wavelength mis-registration of the sun-normalised radiance spectrum with respect to the ozone absorption cross-section spectrum in vacuo, a wavelength shift between the earthshine radiance and direct-sun irradiance spectra, the ozone profile, Ring effect scaling factor,

[1]Artefacts due for example to imperfect radiometric calibration, etalon formed from contamination of optical surfaces not in common for direct-sun and earthshine measurements or un-modelled spectral features in UV surface sun-normalised radiance.

vertical column $NO_2$, BrO and formaldehyde. Other species that absorb in this spectral region (such as $SO_2$) are modelled in the fit (based on a climatological profile shape) but not retrieved.

The retrieved ozone profile is represented in the state-vector as the logarithm of the volume mixing ratio on a fixed pressure grid: surface pressure, 450, 170, 100, 50, 30, 20, 10, 5, 3, 2, 1, 0.5, 0.3, 0.17, 0.1, 0.05, 0.03, 0.017, 0.01 hPa. The forward model performs radiative transfer calculations on a finer pressure grid, and uses the assumption that the log of ozone concentration varies linearly with log pressure between the retrieval levels. The pressure levels are herein conventiently expressed as a pressure-altitude coordinate, where an approximate equivalent altitude is assigned to a pressure profile based on the relation:

$$Z^* = 16(3.0 - \log_{10}(p)) \quad (2)$$

Where $Z^*$ is in km and $p$ in hPa. This predicts approximate equivalent altitudes of the pressure grid of 0, 6 km, 12 km 18 km then every 4 km up to 80 km. These values are usually within 2 km of the geometric altitudes calculated for hydrostatic balance. Altitudes expressed herein are $Z^*$ altitudes. The forward model grid is finer in order to accurately model atmospheric radiative transfer. There are typically 5–6° of freedom for signal (Rodgers, 2000) for the combined Hartley-Huggins bands retrieval. This is almost independent of latitude and season. The retrieval grid over-samples the profiles in terms of the information content of typical GOME-2 measurements so the retrieval is further constrained using a priori correlations (see below).

The ozone a priori profile used is that of the McPeters et al. (2007) climatology derived in part from ozone sondes, which varies by month. The diagonal elements of the a priori error covariance matrix are set to the larger of the climatological % standard deviation and the following values: 0–12 km (100 %), 16 km (30 %), 20–50 km (10 %), 56 km (50 %) and 60–80 km (100 %). In practice, it is these fixed percentage values that apply in the troposphere, except at very high latitudes where the climatological standard deviation is greater. A 6 km Gaussian correlation length is imposed to specify the off-diagonal elements of the a priori covariance for the initial Band 1 step. The retrieved profile and error covariance matrix from the Band 1 step are used as the a priori profile and to define the diagonal elements of the covariance matrix for the Band 2 steps. An 8 km Gaussian correlation length is then applied to further stabilise the Band 2 ozone retrieval in the region of the UTLS.

To achieve photometric signal to noise adequate to retrieve tropospheric ozone information, it is necessary to average Band 2 spectra from eight adjacent GOME-2 ground pixels[2]. Averaging eight Band 2 pixels (2 across-track and 4 along-track) to create a composite pixel of 160 km × 160 km reduces photometric noise by a factor of approximately $1/\sqrt{8}$. For radiative transfer, the scheme uses a version of the GOMETRAN++ (Rozanov, 1997) but with a number of processing speed improvements (which do not degrade numerical accuracy). A polarisation correction based on scalar/vector LIDORT look-up tables is also implemented, as provided by BIRA (Lerot, 2012). The retrieval scheme uses ECMWF Interim Re-analysis meteorological products for temperature and pressure profiles obtained from the ECMWF data server. The solar reference spectrum is that provided by Chance and Kurucz (2010). The ozone absorption cross sections are those derived by Brion et al. (1993, 1998), Daumont et al. (1992), Malicet et al. (1995).

Although cloud may be modelled according to information from GOME-2 measurements in the $O_2$ A-Band (760 nm) or collocated vis/ir imagery from AVHRR/3 on MetOp, for the purposes of this exercise, cloud radiative transfer is not modelled explicitly, and instead an effective Lambertian surface albedo is co-retrieved. With this approach it is expected that the presence of cloud will lead to a negative bias in retrieved ozone, at altitudes below the cloud top, from where there is little information.

[2]This pixel averaging is not necessary to achieve adequate precision on the total column ozone retrieved from the same spectral region.





AMTD
7, 7923–7962, 2014

### 2.2.1 Optimal estimation

The retrieval uses the standard optimal estimation algebra for the non-linear problem (Rodgers, 2000), used widely for deriving atmospheric properties from satellite measurements. An estimate of the state-vector is obtained by combining measurement and prior information in accordance with their respective error covariance matrices. In the case of ozone profile retrieval from nadir UV spectral measurements such as those of GOME-2, the prior constrains what is otherwise an ill-posed problem. The solution is obtained by minimising a cost function, $\chi^2$:

$$\chi^2 = (\boldsymbol{y} - \mathbf{F}(\boldsymbol{x}))^{\mathrm{T}} \mathbf{S}_y^{-1} (\boldsymbol{y} - \mathbf{F}(\boldsymbol{x})) + (\boldsymbol{x}_\mathrm{a} - \boldsymbol{x})^{\mathrm{T}} \mathbf{S}_\mathrm{a}^{-1} (\boldsymbol{x}_\mathrm{a} - \boldsymbol{x}) \tag{3}$$

Where $\boldsymbol{y}$ is the measurement vector, $\boldsymbol{x}$ and $\boldsymbol{x}_\mathrm{a}$ are the state vector (or expected solution) and a priori vector, $\mathbf{F}$ is the forward model and $\mathbf{S}_y$ and $\mathbf{S}_\mathrm{a}$ the error covariance matrices for the measurement and prior, respectively. The Levenburg–Marquardt method is used to minimise the cost function (summarised in Press et al., 1995), and the state vector is iteratively updated as follows:

$$\boldsymbol{x}_{i+1} = \boldsymbol{x}_i + \left(\mathbf{K}_i^{\mathrm{T}} \mathbf{S}_y^{-1} \mathbf{K}_i + \mathbf{S}_\mathrm{a}^{-1} + \gamma \mathbf{I}\right)^{-1} \mathbf{K}_i^{\mathrm{T}} \mathbf{S}_y^{-1} (\boldsymbol{y} - \mathbf{F}(\boldsymbol{x}_i) + \mathbf{K}_i (\boldsymbol{x}_i - \boldsymbol{x}_\mathrm{a})) \tag{4}$$

Where $\gamma$ is the step size, depending upon which the iteration tends towards either Newtonian iteration or steepest descent (Rodgers, 2000). $\mathbf{K}$ is the weighting function at iteration $i$, defined as:

$$\mathbf{K}_i = \frac{\partial \mathbf{F}(\boldsymbol{x}_i)}{\partial \boldsymbol{x}_i} \tag{5}$$

The solution covariance is given by:

$$\mathbf{S}_x = \left(\mathbf{S}_\mathrm{a}^{-1} + \mathbf{K}^{\mathrm{T}} \mathbf{S}_y^{-1} \mathbf{K}\right)^{-1} \tag{6}$$





AMTD
7, 7923–7962, 2014

## 2.3 Improvements to ozone profile retrieval scheme for GOME-2

GOME-2 measurements are subject to measurement errors from a variety of sources, which must be characterized on a pixel-by-pixel basis for accurate retrievals using optimal estimation. As an estimate of the photometric and dark current noise was not supplied with the Level 1b data acquired by GOME-2 before 2013, we use a model to estimate the measurement noise, based on calibration key data derived for the GOME-2 error study (Kerridge et al., 2002) now updated with calibration key data for the MetOp-A GOME-2 instrument, and similar to the model used by Nowlan et al. (2011). The noise model is described in detail in (Miles et al., 2012).

### 2.3.1 Correction for degradation to GOME-2 UV throughput

The MetOp-A GOME-2 instrument (and instruments of its class) is subject to throughput degradation over time that is more acute at the shorter UV wavelengths (Lang et al., 2009; Lacan and Lang, 2011; Cai et al., 2012). To accommodate this, a low-order polynomial fit in wavelength and time has been derived empirically from the ratio between a climatological (in this case the same as the a priori) modelled UV sun-normalised radiance (with its associated solar viewing geometry) and the observed sun-normalised radiance spectrum. This is similar to the approach by van der A (2001) for ozone column retrieval. A detector dark current, or leakage current, in raw signal units, which is assumed constant for all detector pixels in Band 1, has been jointly fit with the low-order polynomial in order to separate the wavelength/time polynomial from this instrumental parameter, since the dark current is co-retrieved with the ozone profile and other parameters from individual Band 1 (Hartley band) measurements. A separate polynomial correction has been derived for each of the West, Nadir and East Band 1 scan positions, sampling only cloud-free data within 30° of the equator one day-per-week throughout the mission. The empirical degradation correction employed in Band 1 has resulted in a relatively stable stratospheric ozone distribution from that Band. A degradation correction has not been applied in the Band 2 (Huggins bands) step and so the retrieval is still sensitive to trends in the total column ozone) although the use of differential structure greatly reduces sensitivity of the Huggins bands retrieval step to UV radiometry. The more subtle effect on ozone retrieval of differential UV degradation (for the irradiance and irradiance) in Band 2 will be a topic of future work.

### 2.3.2 Systematic residual from spectral fit to the Huggins Bands

A systemetic residual spectral signature remains from the Huggins band fit that is of the order of 0.2 % amplitude (of sun-normalised radiance). This signature has a characteristic spectral structure, which is quite persistent not only with sun-earth viewing geometry and time. Although its origins in the solar spectral irradiance, atmosphere/surface (polarised) radiative transfer and/or instrument response have yet to be firmly established, the persistence of the spectral residal is amenable to the co-retrieval of a scaling factor, which enables an RMS fit precision of $< 0.1$ % to then be achieved in the Huggins bands, commensurate with the estimated photometric noise level. In practice, the leading six principle components of the systematic residual spectral signature have been determined (considering fit residuals from observations on selected days spanning the missing to date) and scaling factors for each of these included in the retrieval state vector. Variations of the retrieved scaling factors with both time and space, give some physical insights into their origin and an opportunity for future development.

Although these principle components of the systematic residual signature should not be spectrally-correlated to ozone, some correlation is found between the retrieved scaling factors and tropospheric ozone under conditions that are particularly challenging, such as at high latitudes in the Northern Hemisphere spring, below high columns of stratospheric ozone and where temperature is close isothermal over a broad layer near the tropopause.

Some quality control of the retrieved product is necessary under these cirumstances, where if the line-of-sight zenith angle component of the total column ozone in step 1 (Band 1) is greater than 500 DU, the retrieved tropospheric column is unreliable and the pixel should not be used. These conditions usually coincide with an extensive





AMTD
7, 7923–7962, 2014

near-isothermal tropopause. Since the information on the ozone profile below the stratospheric peak is principally derived from the temperature-dependent ozone spectral structure, such conditions are particularly unfavourable for high precision retrievals in this region.

### 2.3.3 Retrieval of slit function width

In order to achieve the fit precision in the Huggins bands needed to retrieve tropospheric ozone, accurate knowledge of the spectral response function (or slit function) of individual detector pixels is required. The slit functions for the GOME-2 instrument were characterised prior to launch from laboratory measurements (Siddans et al., 2006), but it became apparent while in orbit that they had changed and continue to change (Cai et al., 2012). Failure to adequately characterise the changing slit function leads to a spurious trend (with respect to ozonesondes) in the retrieved ozone; particularly in the troposphere. To account with this, an offline slit function OE retrieval has been added to the fit of daily direct-sun measurement to the high resolution solar reference spectrum (Chance and Kurutz, 2010) which is used to refine wavelength registration (Sect. 2.2). In addition to the series of wavelength polynomial coefficients for radiometric gain, radiometric offset and a wavelength shift/squeeze, the state vector has been extended to incorporate a single scaling factor for the full width half maxima (FWHM) of all the slit functions in the Band 2 wavelength intervalfrom 320–340 nm. This encompasses the wavelength range needed for ozone retrieval and makes an allowance for edge effects from Legendre polynomials. The retrieved FWHM scaling factor is shown in Fig. 1 from January 2007–July 2012. Also shown is an example of how a slit function for a single detector pixel is modified by this parameter, demonstrating the effective narrowing of the slit functions with time in this spectral region. The overall change in FWHM is in good agreement with that suggested by others (e.g. Cai et al., 2012).





AMTD
7, 7923–7962, 2014

## 3 Error analysis and retrieval characterisation

An extensive simulation study of errors pertaining to ozone profile retrieval by the RAL scheme from the GOME-1 UV spectrometer was reported by Siddans, (2003). This was based on retrieval simulations for a set of standard geophysical scenarios which had been defined for the GOME-2 Error Study (Kerridge et al., 2002), which had presented a detailed error budget, based on information available at that time. The retrievals for the GOME-2 instrument in flight is found to behave broadly as predicted.

### 3.1 Retrieval characterisation and error analysis

To ascertain the quality of the retrievals it is necessary to know how they are affected by the contributions of error from non-retrieved or prescribed parameters that contribute to the simulation of the measurement, and therefore the retrieved state.

For a retrieval involving a priori information, the gain matrix **G** (or contribution function), of dimensions $m$ by $n$, where $m$ is the number of measurements (in the sun-normalised radiance spectrum) and $n$ the number of retrieval levels, is defined as follows (Rodgers, 2000):

$$\mathbf{G} = \left(\mathbf{K}^{\mathrm{T}}\mathbf{S}_y^{-1}\mathbf{K} + \mathbf{S}_{\mathrm{a}}^{-1}\right)^{-1}\mathbf{K}^{\mathrm{T}}\mathbf{S}_y^{-1} \tag{7}$$

Where **K** is the weighting function matrix, $\mathbf{S}_y$ the measurement error covariance and $\mathbf{S}_{\mathrm{a}}$ the a priori covariance matrix.

The averaging kernel **A**, an $n$ by $n$ matrix, determines the sensitivity of the retrieval at each level to perturbations in the true atmosphere at every altitude, and therefore shows the vertical smoothing of the retrieval. **A** can calculated from **G** and **K** simply as:

$$\mathbf{A} = \mathbf{GK} \tag{8}$$

Error analyses for the retrieval scheme reported here have been conducted by means of a linear approach, in which perturbations to individual parameters affecting either the





AMTD
7, 7923–7962, 2014

forward model or the measurement are propagated through each of the three retrieval steps to the final solution. This also takes into account that off-diagonals of the ozone prior covariance used in step 3 are different to the solution error covariance output from step 1.

The following equation defines the averaging kernel for the 3-step process:

$$\mathbf{A} = \mathbf{G}_{y3}\mathbf{K}_3 + \mathbf{G}_{a3}\left(\mathbf{M}_1^3\mathbf{A}_1\mathbf{M}_1^{3\mathrm{T}} + \mathbf{M}_2^3\mathbf{A}_2\mathbf{M}_2^{3\mathrm{T}}\right). \tag{9}$$

Where $\mathbf{K}_3$ is the weighting function matrix for step 3, $\mathbf{A}_1$ and $\mathbf{A}_2$ are the averaging kernel matrices for steps 1 and 2 and $\mathbf{G}_{y3}$ and $\mathbf{G}_{a3}$ are the contribution function matrices for step 3 with respect to the measurement vector and a priori vector (Rodgers, 2000).

**M** is the matrix (consisting entirely of "0"s and "1"s) which maps the elements of the state vector at one step (denoted by subscript) into the corresponding element (denoted by the superscript) of the state vector for a later step.

The retrieval precision, or estimated standard deviation ($\sigma$), as given by the square roots of diagonals of the solution error covariance matrix, accounting for photometric, dark current and read-out noise and other quasi-random errors, is generally in the few percent range in the stratosphere increasing to a few 10's of percent in the lowest retrieval levels. From Kerridge et al. (2002) it is expectd that the dominant random error is given by $\sigma$.

The $\sigma$ at each retrieval level of the final step is taken to be the square-root of the diagonal element of the step-3 solution error covariance matrix (which incorporates contributions from the other steps via the step-3 a priori covariance). An example of sub-columns between retrieval levels and the associated errors is given in Fig. 2. As shown in this case, the retrieved sub-column error is typically smaller than the a priori error throughout most of the profile. Figure 3 shows an example of how the $\sigma$ varies for a typical orbit cross section and is also given as a ratio with the prior uncertainty. In general, at all altitudes and latitudes an improvement over the prior uncertainty is observed. An indication of $\sigma$ in the presence of cloud is given later in Sect. 4.





AMTD
7, 7923–7962, 2014

### 3.2 Averaging kernels

Figure 2 also shows example averaging kernels for a mid-latitude ozone profile. The AKs for retrieval levels at the surface and in the mid-troposphere show pronounced peaks in the troposphere, while for higher levels the AKs become smoother. The AKs for retrieval levels in the troposphere have tails which extend much higher; indicating an apparent sensitivity of retrieved tropospheric ozone to true perturbations occurring in the stratosphere and mesosphere. However, variability in ozone number density at those altitudes is in practice very small, and therefore so is its influence on the tropospheric ozone retrieval.

Figure 3 shows a retrieved ozone orbit cross section, the improvement of retrieval error as compared to prior error and the combined surface and 450 hPa AKs. The largest improvement upon prior uncertainty in the example given here is found in the UTLS region at mid to high latitudes, where it is reduced in places to less than 20 % of the prior error. In the tropics, the largest improvement is found in the mid-troposphere. The smallest improvement is found near the surface at high southern latitudes, which in the case of this orbit cross-section coincides with the southern ocean off the south coast of Australia, consistent with the averaging kernels for the lowest levels in the same figure. It is apparent from the AK for the surface retrieval level in Fig. 3 that there is some sensitivity to the lowest 3 km of the atmosphere, although the dominant contribution is from around 500 hPa. Most significantly, this AK has very little contribution from above 10 km and in most circumstances is quite independent of stratospheric ozone. The behaviour of AKs is critical to inter-comparisons with ozonesondes, for validation, and with model distributions, as discussed in the following section.





AMTD
7, 7923–7962, 2014

## 4 Validation and model inter-comparison

In this section the performance of the retrieval algorithm as applied to real measurements will be validated against ozonesondes and inter-compared with the global distribution predicted by a chemistry transport model.

### 4.1 GOME-2 ozonesonde comparison

The period of interest considered here is 2007 (start of mission operations) through 2008. This is principally because some of the characteristics of the instrument changed in September 2009 as a result of an instrument throughput test and it is more straightforward to interpret the results from GOME-2 before that event. The WOUDC/NDACC (Fioletov et al., 2008) and SHADOZ (Thompson et al., 2003) ozonesonde databases are used for this analysis, adopting collocation criteria of $< 200$ km and $< 2$ h, with cloud screening (effective cloud fraction of $< 0.2$ and a cloud top pressure of $> 700$ hPa) unless otherwise stated. All biases are evaluated with respect to the sonde (retrieval minus ozonesonde).

Ozonesonde measurements are known to differ in accuracy with sensor-type, time, altitude and launch site. They are currently the focus of effort by the global ozonesonde community to homogenise the quality of the products (Si$^2$N, 2012). Spurious sondes have been eliminated in this analysis by testing whether each 4 km subcolumn for each sonde site is outside 4$\sigma$ of the monthly mean for that site/subcolumn. This eliminates most abberant sondes whilst retaining characteristic natural variability at the sonde location. Only sondes that extend above 20 km are considered.





AMTD
7, 7923–7962, 2014

#### 4.1.1 Sub-columns and applying averaging kernels

Sonde comparisons are performed in terms of the vertically integrated sub-column between retrieval levels. Sondes are directly integrated using

$$C_i = D \int_{pi}^{pi+1} \boldsymbol{x}(p).\mathrm{d}p \tag{10}$$

Where $C_i$ is the sub-column amount between vertical retrieval grid levels $i$ and $i+1$, $p$ is pressure,

$\boldsymbol{x}$ is ozone mixing ratio, $D$ is a constant such that the resulting sub-columns are in Dobson units. GOME-2 sub-columns are first interpolated onto the forward model grid in a manner consistent with that used in the retrieval (see Sect. 2.2).

Direct comparisons are made between the retrieved and sonde derived sub-columns, however it is also important to account for differences caused by retrieval smoothing using the averaging kernels. These are applied to ozonesonde profiles as described in Deeter et al. (2007), where we apply their Eq. (6) to get an estimate of what the expected retrieved volume mixing ratio (vmr) profile given the sonde profile:

$$\hat{\boldsymbol{x}} = \mathbf{A}^{\mathrm{S}} \left( \boldsymbol{x}^{\mathrm{S}} - \boldsymbol{x}_{\mathrm{a}}^{\mathrm{S}} \right) + \boldsymbol{x}_{\mathrm{a}} \tag{11}$$

Where $\hat{\boldsymbol{x}}$ is the expected simulated retrieval, $\boldsymbol{x}_{\mathrm{a}}$ the a priori profile, $\boldsymbol{x}^{\mathrm{S}}$ and $\boldsymbol{x}_{\mathrm{a}}^{\mathrm{S}}$ are the sonde profile and the a priori profile, defined on the vertical grid at which the sonde profile is provided (indicated by superscript S).

Each row of $\mathbf{A}^{\mathrm{S}}$ characterises the expected perturbation of a given retrieval level to perturbations in the supposed true profile, which is expressed on the relatively finely spaced sonde grid. Retrieval output files contain the (square) mixing ratio averaging kernel $\mathbf{A}$, given directly by Eq. (9), whose rows describe the effect of perturbations on the retrieval grid. The transformation of $\mathbf{A}$ to $\mathbf{A}^{\mathrm{S}}$ (which must account for the different thicknesses of the layers concerned) is achieved by first forming the layer thickness normalised averaging kernel $\mathbf{A}^{\mathrm{N}}$ using:

$$\mathbf{A}^{\mathrm{N}}_{ij} = \mathbf{A}_{ij} \frac{1}{\Delta p_j} \tag{12}$$

Where $\Delta p_j$ is the effective pressure thickness associated with retrieval level $j$:

$$\Delta p_j = \frac{1}{2}\left(p_j + p_{j+1}\right) \tag{13}$$

Here index $i$ refers to rows of the kernel (retrieval levels) while $j$ refers to columns (levels of the true profiles). The rows of $\mathbf{A}^{\mathrm{N}}$ are then linearly interpolated to the vertical grid of the ozonesonde measurement, giving $\mathbf{A}^{\mathrm{N}\prime}$. This is then scaled to give $\mathbf{A}^{\mathrm{S}}$ using

$$\mathbf{A}^{\mathrm{S}}_{ij} = \mathbf{A}^{\mathrm{N}}_{ij} \Delta p^{\mathrm{S}}_j \tag{14}$$

Where $\Delta p^{\mathrm{S}}_j$ is the effective thickness of sonde grid index $j$. Applying Eq. (11) will provide estimated of mixing ratios on the retrieval grid with vertical smoothing consistent with the satellite vertical sensitivity. These are then integrated to give sub-column amounts, in the same way as the retrieved mixing ratios (i.e. by first interpolating to the forward model grid in the appropriate manner).

### 4.1.2 Results

We first consider statistics for an ensemble of all ozonesondes at all sites, and then provide examples in separate latitude bands. Figure 4 shows the bias, standard deviation and correlation coefficient for a priori and retrieved ozone profiles calculated with respect to individual ozonesondes for the full ensemble. The bias is the ensemble average difference between each GOME-2 retrieved profile and the corresponding sonde profile. The fractional bias (also shown) is the bias divided by the mean sonde amount in that layer.





AMTD
7, 7923–7962, 2014

The standard deviation is the ensemble RMS difference between GOME-2 retrievals and corresponding sonde profiles. It is therefore an independent estimate of the (random) error on an individual retrieved profile with respect to the ozonesonde (i.e. ground-truth). The bias, fractional bias and standard deviation are also computed for the a priori profiles. When AKs are applied to the sonde profiles, the retrieval is seen to deliver a substantial improvement on the a priori information, except for the lowest sub-column. This is also the case for the correlation coefficient and is due to atmospheric variability in this lowest layer as sampled by the sondes being generally smaller than $\sigma$. It is therefore important to note that ozone sondes only partially sample the global variabililty (as shown in Sect. 5) The retrieval bias with respect to sondes is rather small once AKs are applied (~6 % in the lowest layer and < 5 % in higher layers), and substantially lower than that of the a priori.

Figure 5 shows that the $\sigma$ provides a good estimate of the retrieval precision in the troposphere, since the subcolumn error ratio ($ER_c$, Eq. 14) of the mean difference between the retrieval and sonde to the estimated error on the retrieved subcolumn is around 1 in all cases, and closer to 1 for the cases where the averaging kernels have been applied.

$$ER_c = \frac{\overline{\left(C_i^{\text{GOME2}} - C_i^{\text{sonde}}\right)}}{\sigma_c} \quad (15)$$

Where $\sigma_c$ denotes the estimated retrieval error for the subcolumn, and the over-bar indicates the mean of the differences. Figure 6 shows the a priori and retrieval biases for sub-columns in Dobson units for different latitude bands as well as for the global average. Sonde agreement varies with latitude for a number of reasons, not least because of the changing vertical gradients and amount of ozone present. For the 450–170 hPa layer, the bias is seen to vary from +3 DU in the 30° S–30° N band to −3 DU in the 30–60° S, 60–90° S and 60–90° N bands. The bias exceeds +5 DU in the 60–90° S band for the 50–30 hPa and 30–20 hPa layers, which is due to the retrieval being influenced



AMTD
7, 7923–7962, 2014

by an a priori profile which is very unrepresentative of ozone hole conditions occurring in the Antarctic spring stratosphere. There is seen to be a small persistent positive bias (+2–3 DU) in the stratosphere (< 100 hPa) in all other latitude bands.

### 4.2 Retrieval performance in the presence of cloud

Retrievals of tropospheric ozone are affected by the presence of cloud. Extensive, thick cloud prevents photons penetrating to lower layers. As discussed in Sect. 2.2, the fitting of a surface albedo in Band 1 (270–308 nm) and in Band 2 (335 nm) partially accommodates cloud sun-normalised radiance and above-cloud scattering, so the remaining impact of cloud is obscuration of the ozone column beneath, as demonstrated in Fig. 7. Cloud information (effective cloud fraction and cloud top pressure) provided in the GOME-2 L1 data for each ground pixel from the FRESCO scheme (Fournier et al., 2004) are provided with the RAL height-resolved ozone product, so as to allow filtering by users.

### 4.3 Comparison to the global chemical transport model TOMCAT

Whereas ozonesondes can provide accurate ground "truth" for validation at a limited number of fixed locations, global chemistry transport models (CTMs) provide geographical and temporal distributions for comparison with satellite data. These are driven by realistic atmospheric circulation (e.g. ECMWF re-analysed winds) and emission inventories, but employ differing schemes for chemistry, surface deposition, boundary layer mixing, convection and other vertical transport processes. Intercomparison of satellite data with a CTM can nonetheless be informative to evaluate both. Here we present a comparison of GOME-2 lower tropospheric ozone with the TOMCAT CTM. We focus our comparison on the lowest layer, which is the most challenging for ozone retrieval from satellite.





AMTD
7, 7923–7962, 2014

### 4.3.1 TOMCAT chemistry transport model

A full description of the TOMCAT Chemistry Transport Model is given elsewhere (Arnold et al., 2005; Chipperfield, 2006 and summarised in Richards et al., 2013), but it is briefly outlined here. TOMCAT is a three-dimensional chemical transport model which is optimised to reproduce the composition of the global troposphere. The version used here has a horizontal resolution of approximately 2.8° × 2.8° and has been driven by ECMWF ERA-Interim temperature, winds and humidity (Dee et al., 2011). It operates on 31 hybrid sigma-pressure levels and the chemistry scheme and emission inventories used in this study are detailed in Richards et al. (2013). The model was spun-up for six months and then global $O_3$ fields were output four times per day at 00:00, 06:00, 12:00 and 18:00 UT. Model fields were interpolated in time and space to the satellite sampling (MetOp has an overpass time of 09:30 LT) for 2008. Lower tropospheric ozone retrieved from GOME-2 by the RAL scheme has previously been shown to have excellent agreement with TOMCAT, in particular for the NH summer Mediterranean region (Richards et al., 2013).

### 4.3.2 Model comparison

Figure 8 compares GOME-2 with TOMCAT for the lowest retrieved subcolumn in August 2008. The GOME-2 data have been cloud-screened, based on cloud height and fraction from FRESCO in the L1b data, and GOME-2 AKs have been applied to the model. Geographical structure in the monthly-mean distribution is seen to be represented quite consistently by GOME-2 and the model. In particular, there is seen to be agreement in locations of high ozone concentration over the Mediterannean region and south-east China, which are typically found at this time of year, although peak values observed there by GOME-2 are higher than predicted by TOMCAT.

Consistency between GOME-2 and TOMCAT geographical distributions is indicated quantitatively by the standard deviation (4 DU) and correlation coefficient (0.66) for the August 2008 ensemble in Fig. 8. The global mean bias between GOME-2 and TOMCAT





AMTD
7, 7923–7962, 2014

(∼ 0.8 DU) for August 2008 is comparable to that between GOME-2 and ozonsondes in this layer (∼ 1 DU) for the two-years 2007–2008. Furthermore, the latitudinal dependence of the GOME-2 minus TOMCAT difference in Fig. 8 also mirrors that of the GOME-2 minus ozonesonde bias in Fig. 5; being positive at northern mid/high-latitudes and negative at southern mid-latitudes.

### 4.3.3 Model timeseries comparison

Figure 9 shows monthly mean averages for the GOME-2 retrieval and its a priori, and the TOMCAT model (with GOME-2 spatial sampling) in four regions. These are the NH remote Pacific, USA, Mediterrannean and Eastern China. The remote Pacific in particular is not well sampled by ozonesondes. In the four regions selected, there is good agreement between GOME-2 and TOMCAT in the shape of the seasonal cycle in lower tropospheric ozone. This is particularly the case for USA and Eastern China, where a double peak in the seasonal cycles is seen by both the model and the retrieval, but not the a priori. In the Mediterranean, the summer peak is found to occur at a similar time in the retrieval and model but several months earlier in the prior.

## 5 Summary

The RAL ozone profile retrieval algorithm for nadir-viewing satellite UV spectrometers has been developed to have sensitivity to tropospheric as well as stratospheric ozone. This has been achieved by a three-step retrieval approach in which high fit precision (< 0.1 % RMS) is required in the third step to extract tropospheric information from the temperature dependent Huggins bands (323–335 nm). The bias with respect to ozonesondes sampled worldwide over two years is of the order of 6 % (∼ 1 DU) in the surface 450 hPa layer and < 5 % in the sub-columns above. The bias in part reflects the extent to which uncertainties in knowledge of the GOME-2 absolute UV (Hartley band) radiometry and (Huggins bands) slit function shape can be accommodated. The





AMTD
7, 7923–7962, 2014

bias varies systematically with latitude/solar zenith angle. It is typically less than ±3 DU, except in the tropical UTLS region where there is a positive bias of up to a 5 DU, due to smearing of the sharp change in ozone vertical gradient near the tropopause. This corresponds to less than ±20 % in the troposphere and +10 % in the tropical UTLS. As expected, the retrieval shows a negative bias in the troposphere in the presence of high or pervasive cloud because, for this validation exercise, cloud parameters have not been co-retrieved or explicitly modelled; their effects on UV sun-normalised radiance have been accommodated only through retrieval of an effective Lambertian albedo (and no ghost column has been added).

The GOME-2 retrieval and the chemistry transport model TOMCAT show agreement in the August 2008 monthly-mean global distribution of lower tropospheric ozone and specifically in the location of high ozone concentrations over the Mediterranean and over south-east China. Concentrations in the surface-450 hPa layer retrieved from GOME-2 are persistently higher at northern mid/high latitudes and lower at southern mid-latitudes than predicted by TOMCAT; a pattern which is consistent with the GOME-2-ozonesonde bias for 2007–2008.

Significant improvements to the UV GOME-2 retrieval scheme are now planned. These include: (a) updating to and valuating performance with the latest spectroscopy (e.g. Surdyuchenko et al., 2014); (b) improved modelling of the slit function shape and related changes with time; (c) improved handling of radiometric degradation occurring in both the Hartley and Huggins bands over the mission lifetime and (d) addition of the visible (Chappuis) bands as a 4th retrieval step, to increase ozone sensitivity in the lower troposphere over land. We would also wish to remove the retrieval of an ozone absorption cross-section shift which should add significant information.

*Acknowledgements.* This work is funded by the Natural Environment Research Council's (NERC) through the National Centre for Earth Observation (NCEO), and in part also by ESA Climate Change Initiative and EUMETSAT Visiting Scientist Position in O3MSAF).





AMTD
7, 7923–7962, 2014

## References


Arnold, S. R., Chipperfield, M. P., and Blitz, M. A.: A three dimensional model study of the effect of new temperature dependent quantum yields for acetone photolysis, J. Geophys.Res.-Atmos., 110, D22305 doi:10.1029/2005jd005998, 2005.

Boynard, A., Clerbaux, C., Coheur, P.-F., Hurtmans, D., Turquety, S., George, M., Hadji-Lazaro, J., Keim, C., and Meyer-Arnek, J.: Measurements of total and tropospheric ozone from IASI: comparison with correlative satellite, ground-based and ozonesonde observations, Atmos. Chem. Phys., 9, 6255–6271, doi:10.5194/acp-9-6255-2009, 2009.

Bhartia, P. K., McPeters, R. D., Mateer, C. L., Flynn, L. E., and Wellemeyer, C.: Algorithm for the estimation of vertical ozone profiles from the backscattered ultraviolet technique, J. Geophys. Res., 101, 18793–18806, doi:10.1029/96JD01165, 1996.

Brinksma, E. J., Bracher, A., Lolkema, D. E., Segers, A. J., Boyd, I. S., Bramstedt, K., Claude, H., Godin-Beekmann, S., Hansen, G., Kopp, G., Leblanc, T., McDermid, I. S., Meijer, Y. J., Nakane, H., Parrish, A., von Savigny, C., Stebel, K., Swart, D. P. J., Taha, G., and Piters, A. J. M.: Geophysical validation of SCIAMACHY Limb Ozone Profiles, Atmos. Chem. Phys., 6, 197–209, doi:10.5194/acp-6-197-2006, 2006.

Brion, J., Chakir, A., Daumont, D., and Malicet, J.: High-resolution laboratory absorption cross section of O3: Temperature effect, Chem. Phys. Lett., 213, 610–512, 1993.

Brion, J., Chakir, A., Charbonnier, J., Daumont, D., Parisse, C., and Malicet, J.: Absorption spectra measurements for the ozone molecule in the 350–830 nm region, J. Atmos. Chem., 30, 291–299, 1998.

Cai, Z., Liu, Y., Liu, X., Chance, K., Nowlan, C. R., Lang, R., Munro, R., and Suleiman, R.: Characterization and correction of Global Ozone Monitoring Experiment 2 ultraviolet measurements and application to ozone profile retrievals, J. Geophys. Res., 117, D07305, doi:10.1029/2011JD017096, 2012.

Callies, J., Corpaccioli, E., Eisinger, M., Hahne, A., and Lefebvre, A.: GOME-2 – Metop's Second-Generation, Sensor for Operational Ozone Monitoring, ESA Bull.-Eur. Space, 102, 28–36, 2000.

Chance, K. and Kurucz, R. L.: An improved high-resolution solar reference spectrum for Earth's atmosphere measurements in the ultraviolet, visible, and near infrared, J. Quant. Spectrosc. Ra., 111, 1289–1295, 2010.

Chipperfield, M. P.: New version of the TOMCAT/SLIMCAT offline chemical transport model: Intercomparison of stratospheric tracer experiments, Q. J. Roy. Meteor. Soc., 132, 1179–1203, doi:10.1256/qj.05.51, 2006.

Daumont, M., Brion, J., Charbonnier, J., and Malicet, J.: Ozone UV spectroscopy I: absorption cross-sections at room temperature, J. Atmos. Chem., 15, 145–155, 1992.

Dee, D. P., Uppala, S. M., Simmons, A. J., Berrisford, P., Poli, P., Kobayashi, S., Andrae, U., Balmaseda, M. A., Balsamo, G., Bauer, P., Bechtold, P., Beljaars, A. C. M., van de Berg, L., Bidlot, J., Bormann, N., Delsol, C., Dragani, R., Fuentes, M., Geer, A. J., Haimberger, L., Healy, S. B., Hersbach, H., Hólm, E. V., Isaksen, L., Kållberg, P., Köhler, M., Matricardi, M., McNally, A. P., Monge-Sanz, B. M., Morcrette, J.-J., Park, B.-K., Peubey, C., de Rosnay, P., Tavolato, C., Thépaut, J.-N., and Vitart, F.: The ERA-Interim reanalysis: configuration and performance of the data assimilation system, Q. J. Roy. Meteor. Soc., 137, 553–597, doi:10.1002/qj.828, 2011.

Deeter, M. N., Edwards, D. P., Gille, J. C., and Drummond, J. R.: Sensitivity of MOPITT observations to carbon monoxide in the lower troposphere, J. Geophys. Res., 112, D24306, doi:10.1029/2007JD008929, 2007.

European Organisation for the Exploitation of Meteorological Satellites (EUMETSAT): GOME-2 Level 1 Product Generation Specification Report, EPS.SYS.SPE.990011, Darmstadt, Germany, 2006.

Fiotov, V. E., Labow, G. J., Evans, T., Hare, E. W., Köhler, U., McElroy, C. T., Miyagawa, K., Redonda, A., Savastiouk, V., Shalamyansky, A. M., Staehelin, J., Vanicek, K., and Weber, M.: Performance of the ground-based total ozone network assessed using satellite data, J. Geophys. Res., 113, D14313, doi:10.1029/2008JD009809, 2008.

Fishman, J. and Larsen, J. C.: Distribution of total ozone and stratospheric ozone in the tropics: implications for the distribution of tropospheric ozone, J. Geophys. Res., 92, 6627–6634, doi:10.1029/JD092iD06p06627, 1987.

Fournier, N., Stammes, P, Acarreta, J. R., and van Geffen, J.: FRESCO Cloud Algorithm for GOME-2, Final Report, ESTEC contract number 17332/03/NL/GS, 2004.

Glatthor, N., von Clarmann, T., Fischer, H., Funke, B., Gil-López, S., Grabowski, U., Höpfner, M., Kellmann, S., Linden, A., López-Puertas, M., Mengistu Tsidu, G., Milz, M., Steck, T., Stiller, G. P., and Wang, D.-Y.: Retrieval of stratospheric ozone profiles from MIPAS/ENVISAT limb emission spectra: a sensitivity study, Atmos. Chem. Phys., 6, 2767–2781, doi:10.5194/acp-6-2767-2006, 2006.

Gryparis, A., Forsberg, B., Katsouyanni, K., Analitis, A., Touloumi, G., Schwartz, J., Samoli, E., Medina, S., Anderson, H. R., Niciu, E. M., Wichmann, H. E., Kriz, B., Kosnik, M., Skorkovsky, J., Vonk, J. M., and Dortbudak, Z.: Acute effects of ozone on mortality from the "Air pollution and health: a European approach" project, Am. J. Resp. Crit. Care Med., 170, 1080–1087, doi:10.1164/rccm.200403-333OC, 2004.

Hollaway, M. J., Arnold, S. R., Challinor, A. J., and Emberson, L. D.: Intercontinental transboundary contributions to ozone-induced crop yield losses in the Northern Hemisphere, Biogeosciences, 9, 271–292, doi:10.5194/bg-9-271-2012, 2012.

Joiner, J., Barthia, P. K., Cebula, R. P., Hilsenrath, E., McPeters, R. D., and Park, H.: Rotational Raman scattering (ring effect) in satellite backscatter ultraviolet measurements, Appl. Optics, 34, 4513–4525, 1995.

Keppens, A., Lambert, J.-C., Granville, J., Hubert, D., Verhoelst, T., Miles, G., Siddans, R., van Peet, J., van der A, R., Delcloo, A., Godin-Beekmann, S., Kivi, R., Stübi, R., Munro, R., and Zehner, C.: Round-Robin evaluation of nadir ozone profile retrievals: methodology and application to MetOp-A GOME-2, Atmos. Meas. Tech. Discuss., submitted, 2014.

Kerridge, B. J. K., Siddans, R., Latter, B. L., Burrows, J. P., Weber, M., De Beek, R., Aben, I., and Hartman, W.: GOME-2 Error Assessment Study, Final Report EUMETSAT Contract No EUM/CO/01/901/DK, 2002.

Klenk, K. F., Bhartia, P. K., Fleig, A. J., Kaveeshwar, V. G., McPeters, R. D., and Smith, P. M.: Total ozone determination from the Backscattered Ultraviolet (BUV) experiment, J. Appl. Meteorol., 21, 1672–1684, 1982.

Lacan, A. and Lang, R.: Investigation on GOME-2 throughput degradation, Final report, EUM/LEO/REP/09/0732 Issue 1.1, 16 July 2011.

Lang, R., Munro, R., Livschitz, Y., Dyer, R., and Lacan, A.: GOME-2 FM3 Long-Term In-Orbit Degradation – Basic Signatures After 2nd Throughput Test, EUMETSAT Technical report, EUM.OPS-EPS.DOC.09.0464, 2009.

Lerot, C.: Personal communication, 2012.

Liu, X., Chance, K., Sioris, C. E., Spurr, R. J. D., Kurosu, T. P., Martin, R. V., and Newchurch, M. J.: Ozone profile and tropospheric ozone retrievals from Global Ozone Monitoring Experiment: algorithm description and validation, J. Geophys. Res., 110, D20307, doi:10.1029/2005JD006240, 2005.

Liu, X., Bhartia, P. K., Chance, K., Spurr, R. J. D., and Kurosu, T. P.: Ozone profile retrievals from the Ozone Monitoring Instrument, Atmos. Chem. Phys., 10, 2521–2537, doi:10.5194/acp-10-2521-2010, 2010.

Loyola, D. G., Koukouli, M. E., Valks, P., Balis, D. S., Hao, N., Van Roozendael, M., Spurr, R. J. D., Zimmer, W., Kiemle, S., Lerot, C., and Lambert, J.-C.: The GOME-2 total column ozone product: Retrieval algorithm and ground-based validation, J. Geophys. Res., 116, D07302, doi:10.1029/2010JD014675, 2011.

Livesey, N. J., Read, W. G., Filipiak, M. J., Froidevaux, L., Harwood, R. S., Jiang, J. H., Jimenez, C., Pickett, H. M., Pumphrey, H. C., Santee, M. L., Schwartz, M. J., Waters, J. W., and Wu, D. L.: Earth Observing System (EOS) Microwave Limb Sounder (MLS) Version 1.5 Level 2 data quality and description document, Tech. Rep. JPL D-32381, Jet Propulsion Laboratory, California Institute of Technology, Pasadena, CA, 2005.

Malicet, C., Daumont, D., Charbonnier, J., Parisse, C., Chakir, A., and Brion, J.: Ozone UV spectroscopy, II. Absorption cross-sections and temperature dependence, J. Atmos. Chem., 21, 263–273, 1995.

McPeters, R. D., Lebow, G. J., and Logan, J. A.: Ozone climatological pro?les for satellite retrieval algorithms, J. Geophys. Res., 112, D05308, doi:10.1029/2005JD006823, 2007.

Miles, G. M., Siddans, R. S., Tuinder, O., and Latter, B. L.: Analysis of GOME-2 Level-1b Data Quality and Degradation Effects on Operational Ozone Profile Retrievals, EUMETSAT O3MSAF Visiting Scientist Final Report, 2012.

Munro, R., Siddans, R., Reburn, W. J., and Kerridge, B. J.: Direct measurement of tropospheric ozone distributions from space, Nature, 392, 168–171, doi:10.1038/32392, 1998.

Nassar, R., Logan, J. A., Worden, H. M., Megretskaia, I. A., Bowman, K. W., Osterman, G. B., Thompson, A. M., Tarasick, D. W., Austin, S., Claude, H., Dubey, M. K., Hocking, W. K., Johnson, B. J., Joseph, E., Merrill, J., Morris, G. A., Newchurch, M., Oltmans, S. J., Posny, F., Schmidlin, F. J., Vomel, H., Whiteman, D. N., and Witte, J. C.: Validation of Tropospheric Emission Spectrometer (TES) nadir ozone profiles using ozonesonde measurements, J. Geophys. Res.-Atmos., 113, D15s17, doi:10.1029/2007jd008819, 2008.

Nowlan, C. R., Liu, X., Chance, K., Cai, Z., Kurosu, T. P., Lee, C., and Martin, R. V.: Retrievals of sulfur dioxide from the Global Ozone Monitoring Experiment 2 (GOME-2) using an optimal estimation approach: algorithm and initial validation, J. Geophys. Res., 116, D18301, doi:10.1029/2011JD015808, 2011.





AMTD
7, 7923–7962, 2014

O3MSAF: O3M SAF Validation Report for Near-Real-Time Ozone Profile, Offline Ozone Profile, Near-Real-Time High Resolution Ozone Profile and Offline High Resolution Ozone Profile products, SAF/O3M/RMI&DWD/VR/001, 2013.

Platt, U.: Differential optical absorption spectroscopy (DOAS), Chem. Anal., 127, 27–83, 1994.

Plumber, S.: The ESA Climate Change Initiative – Description, Technical Note: EOP-SEP/TN/0030-09/SP, ESA, 2009.

Press, W. H., Teukolksy, S., Vetterling, W. T., and Flannery, B.: Numerical Recipes: the Art of Scientific Computing, 2nd edn., Cambridge University Press, 1995.

Richards, N. A. D., Arnold, S. R., Chipperfield, M. P., Miles, G., Rap, A., Siddans, R., Monks, S. A., and Hollaway, M. J.: The Mediterranean summertime ozone maximum: global emission sensitivities and radiative impacts, Atmos. Chem. Phys., 13, 2331–2345, doi:10.5194/acp-13-2331-2013, 2013.

Rodgers, C. D.: Retrieval of atmospheric temperature and composition from remote measurements of thermal radiation, Rev. Geophys. Space Ge., 14, 609–624, doi:10.1029/RG014i004p00609, 1976.

Rodgers, C. D.: Inverse Methods for Atmospheric Sounding: Theory and Practice, World Sci., Hackensack, NJ, 2000.

Rozanov, V. V., Diebel, D., Spurr, R. J. D., and Burrows, J. P.: GOMETRAN: a radiative transfer model for the satellite project GOME – the plane-parallel version, J. Geophys. Res., 102, 16683–16695, 1997.

Schoeberl, M. R., Ziemke, J. R., Bojkov, B. et al.: A trajectory-based estimate of the tropospheric ozone column using the residual method, J. Geophys. Res., 112, D24S49, doi:10.1029/2007JD008773, 2007.

Siddans, R.: Height Resolved Ozone Retrievals from Global Ozone Monitoring Experiment, PhD Thesis, University of Reading, 2003.

Siddans, R., Kerridge, B. J., Latter, B. G., Smeets, J., Otter, G., and Slijkhuis, S.: Analysis of GOME-2 Slit Function Measurements: Final Report, EUM/CO/04/1298/RM, Eur. Organ. for the Exploit. of Meteorol. Satell., Darmstadt, Germany, 2006.

$SI^2N$ (SPARC/IO3C/IGACO-O3/NDACC) Initiative: Activity on Past Changes in the Vertical Distribution of Ozone, available at: http://igaco-o3.fmi.fi/VDO/index.html (last access: 28 July 2014), 2011.

Sofieva, V. F., Rahpoe, N., Tamminen, J., Kyrölä, E., Kalakoski, N., Weber, M., Rozanov, A., von Savigny, C., Laeng, A., von Clarmann, T., Stiller, G., Lossow, S., Degenstein, D.,





AMTD

7, 7923–7962, 2014

Tropospheric ozone and ozone profiles retrieved from GOME-2 and their validation

G. M. Miles et al.

Bourassa, A., Adams, C., Roth, C., Lloyd, N., Bernath, P., Hargreaves, R. J., Urban, J., Murtagh, D., Hauchecorne, A., Dalaudier, F., van Roozendael, M., Kalb, N., and Zehner, C.: Harmonized dataset of ozone profiles from satellite limb and occultation measurements, Earth Syst. Sci. Data, 5, 349–363, doi:10.5194/essd-5-349-2013, 2013.

Stocker, T. F., Qin, D., Plattner, G.-K., Tignor, M., Allen, S. K., Boschung, J., Nauels, A., Xia, Y., Bex, V., and Midgley, P. M. (eds.): Climate Change 2013: the Physical Science Basis, Contribution of Working Group I to the Fifth Assessment Report of the Intergovernmental Panel on Climate Change, Cambridge University Press, Cambridge, UK and New York, NY, USA, 1535 pp., 2013.

Serdyuchenko, A., Gorshelev, V., Weber, M., Chehade, W., and Burrows, J. P.: High spectral resolution ozone absorption cross-sections – Part 2: Temperature dependence, Atmos. Meas. Tech., 7, 625–636, doi:10.5194/amt-7-625-2014, 2014.

Thompson, A. M., Witte, J. C., McPeters, R. D., Oltmans, S. J., Schmidlin, F. J., Logan, J. A., Fujiwara, M., Kirchhoff, V. W. J. H., Posny, F., F., Coetzee, G. J. R., Hoegger, B., Kawakami, S., Ogawa, T., Johnson, B. J., Vomel H., and Labow, G. J.: Southern Hemisphere Additional Ozonesondes (SHADOZ) 1998–2000 tropical ozone climatology: 1. comparison with Total Ozone Mapping Spectrometer (TOMS) and ground-based measurements, J. Geophys. Res., 108, 8238, doi:10.1029/2001JD000967, 2003.

van der A, R.: Recalibration of GOME Spectra for the Purpose of Ozone Profile Retrieval, KNMI Technical Note RT-236, 2001.

van Roozendael, M., Spurr, R., Loyola, D., Lerot, C., Balis, D., Lambert, J.-C., Zimmer, W., van Gent, J., van Geffen, J., Koukouli, M., Granville, J., Doicu, A., Otto, S., Fayt, C., and Zehner, C.: Sixteen years of GOME/ERS2 total ozone data: the new direct-fitting GOME Data Processor (GDP) version 5 – algorithm description, J. Geophys. Res., 117, D03305, doi:10.1029/2011JD016471, 2012.

Valks, P., Hao, N., Gimeno Garcia, S., Loyola, D., Dameris, M., Jöckel, P., and Delcloo, A.: Tropical tropospheric ozone column retrieval for GOME-2, Atmos. Meas. Tech. Discuss., 7, 727–768, doi:10.5194/amtd-7-727-2014, 2014.

Zawodny, J. M. and McCormick, M. P.: Stratospheric Aerosol and Gas Experiment II measurements of the quasi-biennial oscillations in ozone and nitrogen dioxide, J. Geophys. Res., 96, 9371–9377, doi:10.1029/91JD00517, 1991.





AMTD
7, 7923–7962, 2014

Ziemke, J. R., Chandra, S., Labow, G. J., Bhartia, P. K., Froidevaux, L., and Witte, J. C.: A global climatology of tropospheric and stratospheric ozone derived from Aura OMI and MLS measurements, Atmos. Chem. Phys., 11, 9237–9251, doi:10.5194/acp-11-9237-2011, 2011.

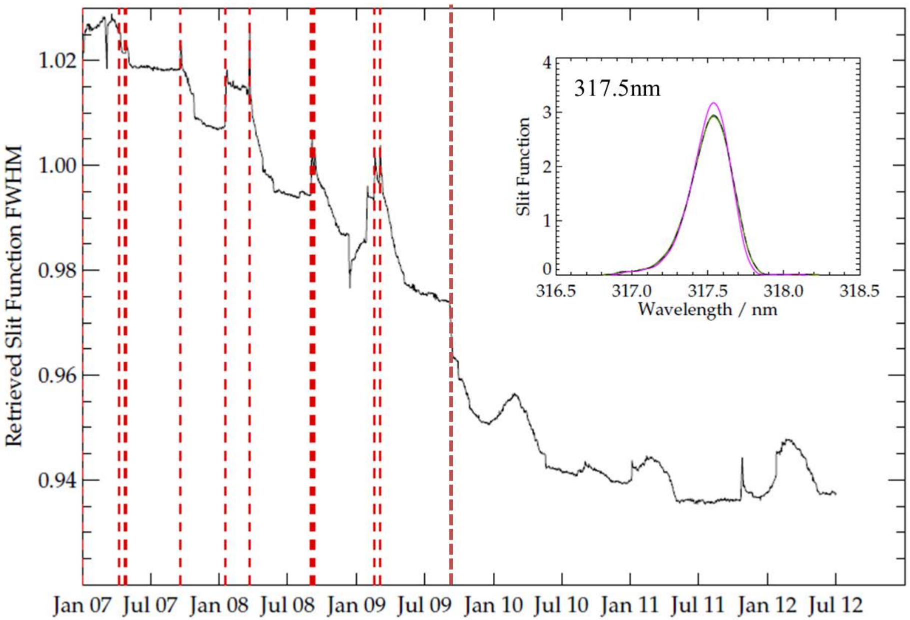


**Figure 1.** Retrieved scaling factor for nominal FWHM of slit function with time (black solid). Red dashed lines indicate discontinuities in trend associated with variaous in-orbit oprations, including the second (and last) throughput test in Septermber 2009. The inset panel shows an example of how the effective shape of the measured slit function is modified for the pixel centred at 317.5 nm, where the black and green lines indicate start of operations and 1 month hense (January and February 2007) and the pink line is the effective shape in January 2013.





AMTD
7, 7923–7962, 2014

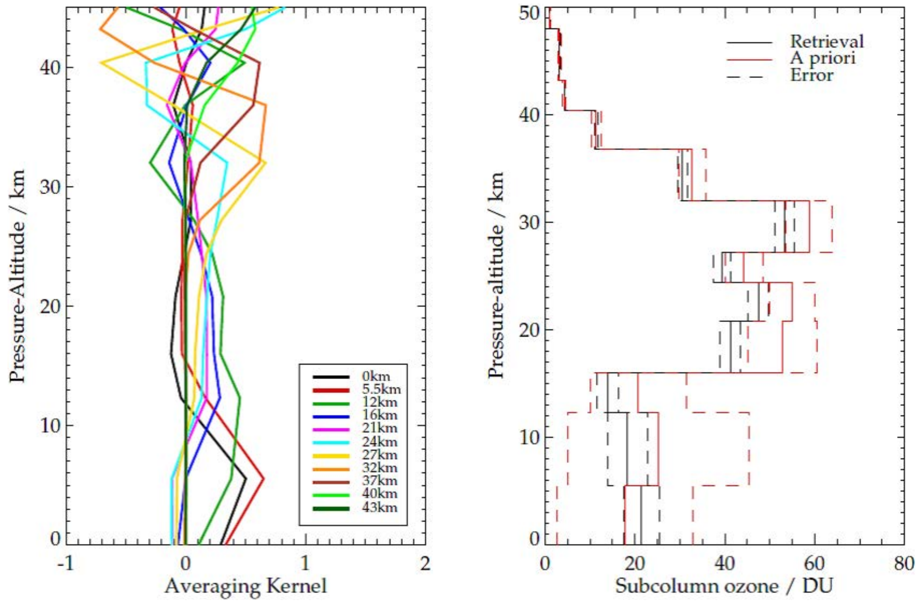


**Figure 2.** The left panel shows averaging kernels in number density units on levels for a nadir pixel at 45° N on 25 August 2008. The right panel shows the associated retrieved and a priori sub-columns and associated errors for this profile.





AMTD
7, 7923–7962, 2014

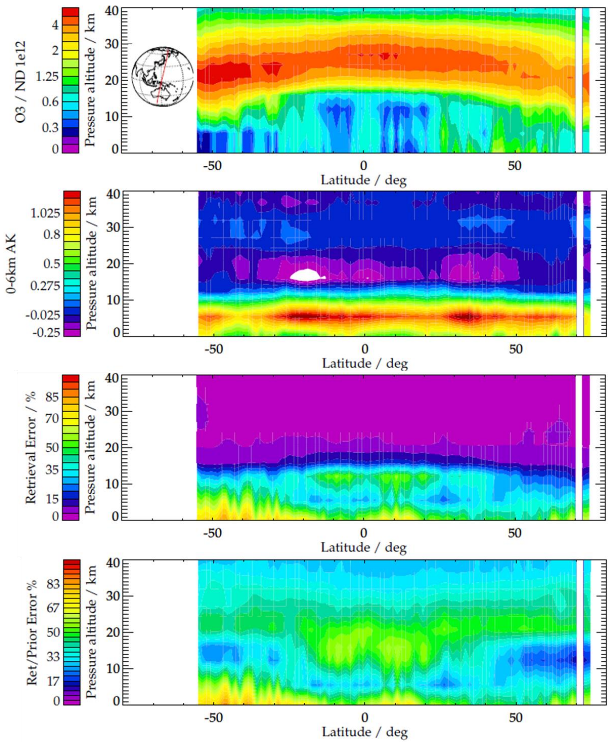


**Figure 3.** The top panel shows an ozone cross-section on 25 August 2008 retrieved from the Band 2 (final) step for the nadir pixel. The orbit track is also indicated. The second panel shows the combined surface and 450 hPa (circa 0 and 6 km) averaging kernels. The third panel show the relative retrieval error. The bottom panel shows the associated ratio of retrieved to a priori error.





AMTD

7, 7923–7962, 2014

Tropospheric ozone and ozone profiles retrieved from GOME-2 and their validation

G. M. Miles et al.

Title Page
Abstract | Introduction
Conclusions | References
Tables | Figures
◀| |▶
◀ ▶
Back | Close
Full Screen / Esc
Printer-friendly Version
Interactive Discussion

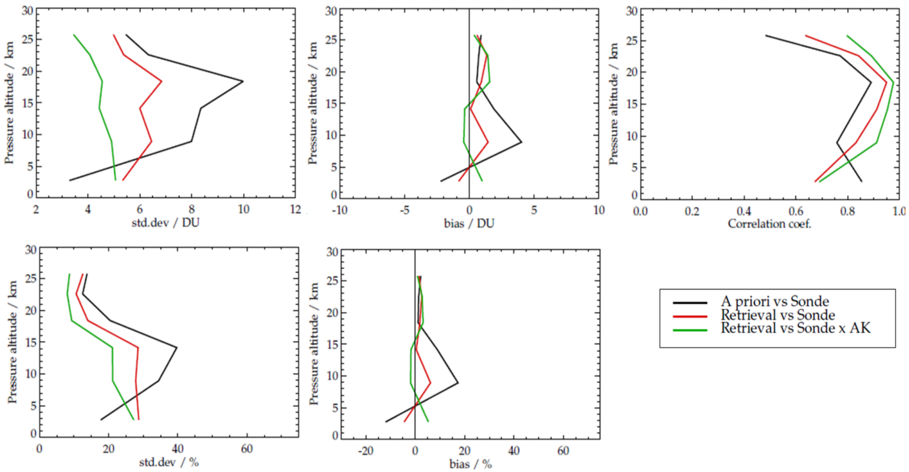


**Figure 4.** Statistical comparison of RAL GOME-2 ozone profiles with ozonesondes sampled worldwide for 2007–2008. Collocation criteria are given in the text. The standard deviations (left) and biases (centre) in GOME-2 minus ozonesonde values are in absolute (DU) units and as % of sonde value in the top and bottom rows, respectively. The top right panel shows the correlation coefficient. Points denote the mid-point of each sub-column. In each case, results are shown for the a priori vs. sonde and for the retrieval vs. sonde with and without application of AKs to the ozonesonde profiles. Statistics have been derived from percentage difference calculated with respect to each individual ozonesonde.





AMTD
7, 7923–7962, 2014

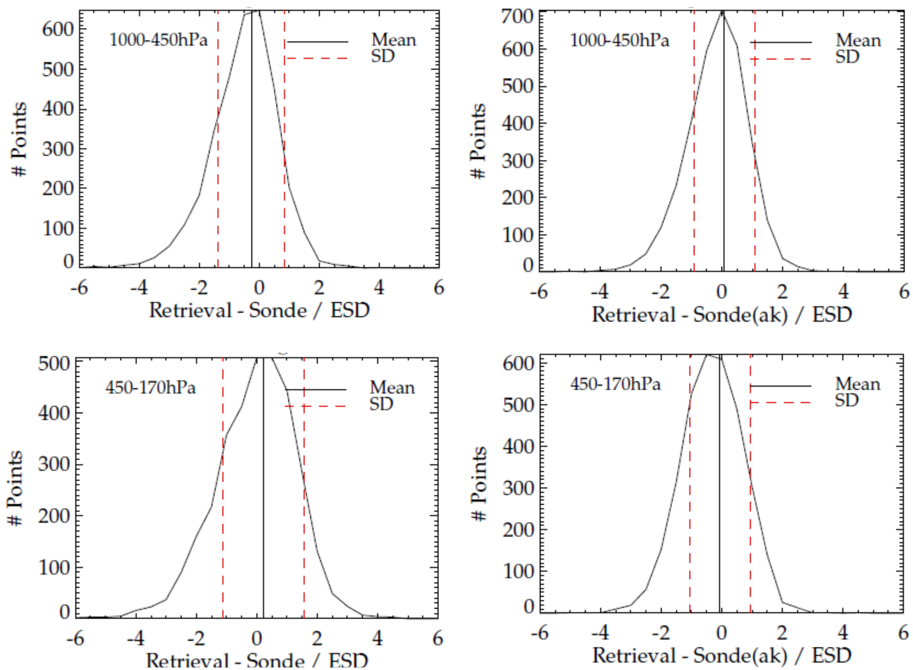


**Figure 5.** Histograms of retrieved difference from sonde relative to the estimated retrieval error ($\sigma_c$) for the lower-most and second sub-columns (top and bottom), with and without averaging kernels applied (right and left).



Discussion Paper | Discussion Paper | Discussion Paper | Discussion Paper |

AMTD
7, 7923–7962, 2014

Tropospheric ozone and ozone profiles retrieved from GOME-2 and their validation

G. M. Miles et al.

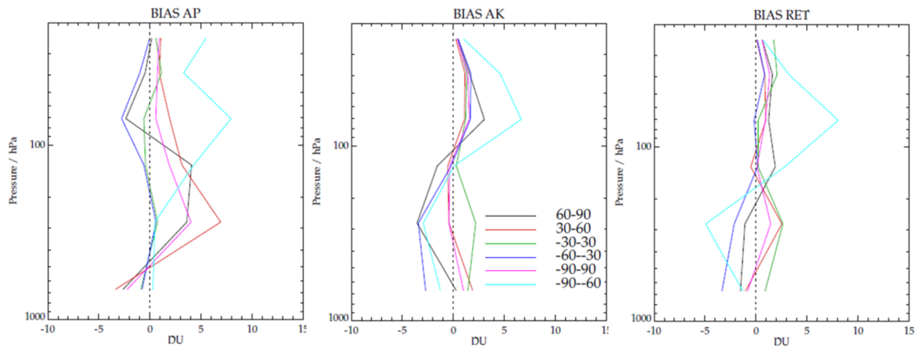


**Figure 6.** Bias with respect to ozonesondes as a function of latitude and pressure for sub-columns in Dobson units for the a priori (left) and retrieved profile (centre) and with GOME-2 AKs applied to the sonde (right). The pink lines indicate the averages over all latitude bands, for comparison to the black and green lines in the left hand panel of Fig. 4, which depict the same a priori and retrieval biases as % differences from the ozonesondes.





AMTD
7, 7923–7962, 2014

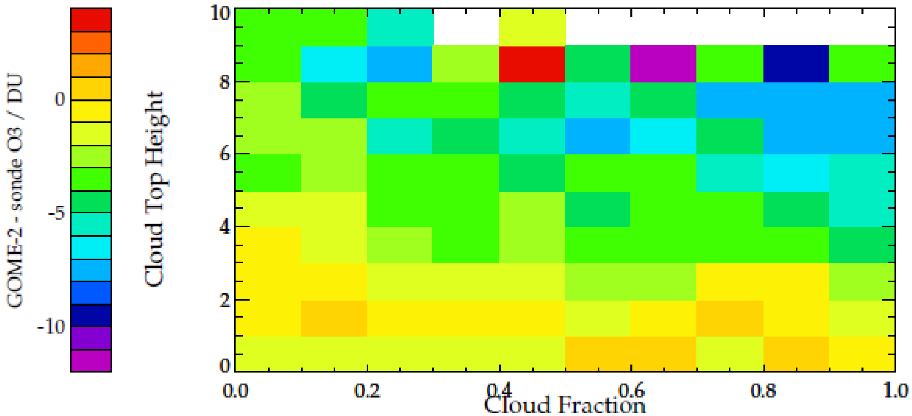


**Figure 7.** The lowest sub-column ozone (surface to 450 hPa) differenced from ozonesonde sub-column (without AKs applied) with no cloud clearing.





AMTD
7, 7923–7962, 2014

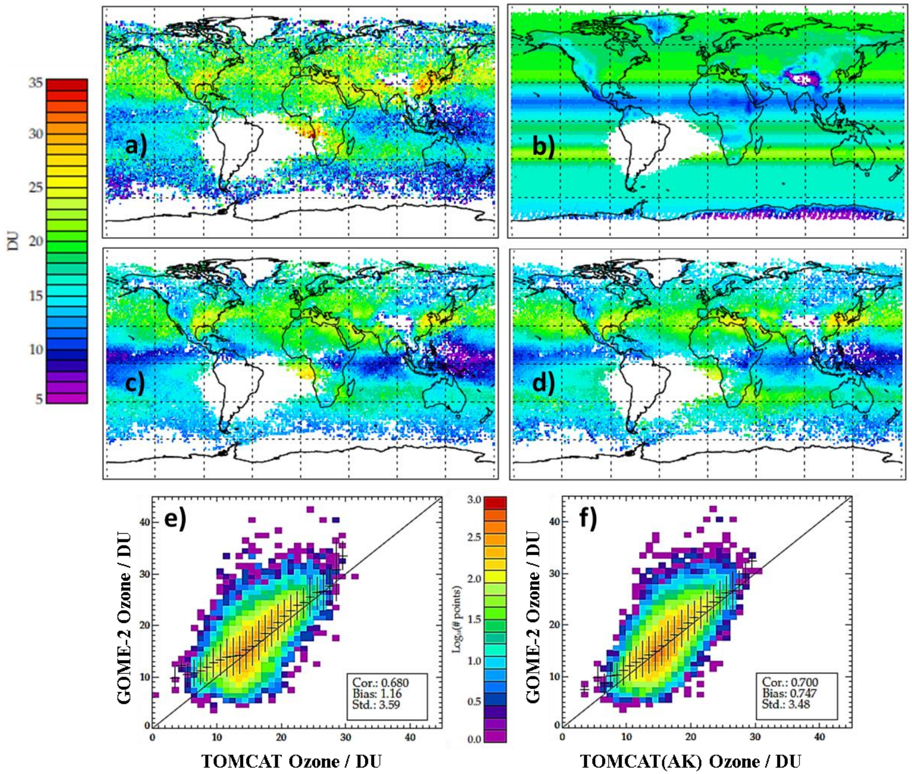


**Figure 8. (a)** GOME-2 Surface to 450 hPa layer ozone gridded (1.125) monthly-mean for September 2008. Pixels have been strictly cloud cleared such that only pixels with a cloud fraction of < 0.2 *and* cloud top pressure of > 700 hPa remain, **(b)** A priori for GOME-2 retrieval (all pixels), **(c)** TOMCAT model with satellite sampling, **(d)** TOMCAT model with GOME-2 averaging kernels applied, **(e)** correlation of a and c with associated bias and standard deviation, **(f)** correlation of **(a)** and **(d)**. The vertical and horizontal black lines in panels **(e)** and **(f)** indicate the respective standard devation of those data sampled at each axes points.





AMTD
7, 7923–7962, 2014

Tropospheric ozone and ozone profiles retrieved from GOME-2 and their validation

G. M. Miles et al.

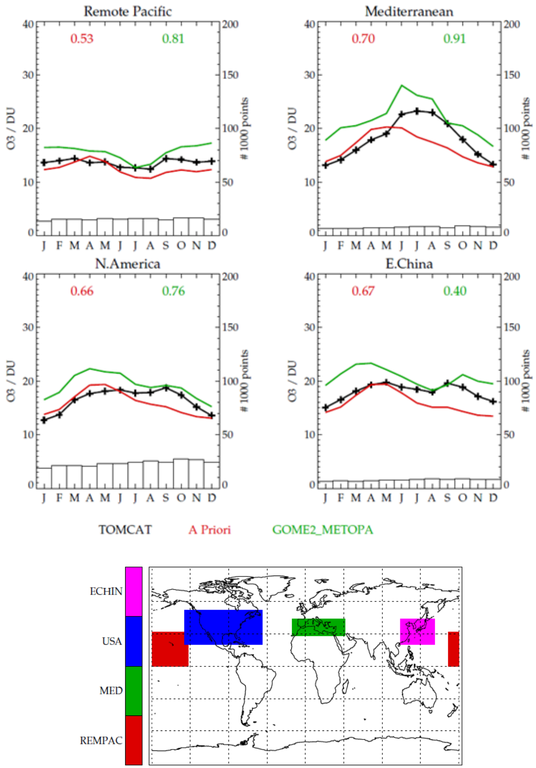


**Figure 9.** Timeseries comparison of surface to 450 hPa ozone for 4 regions of TOMCAT (black), GOME-2 (green) and the GOME-2 retrieval a priori/climatology in 2008. Monthly correlation coefficient of TOMCAT and the a priori (red) and GOME-2 (green) are also given for each region. In all cases GOME-2 averaging kernels have been applied to TOMCAT. Bars and second axis indicate number of measurments in each month for each region.